Available online at www.sciencedirect.com
ScienceDirect
Journal of Theoretical Biology 252 (2008) 173–183
Journal of Theoretical Biology
www.elsevier.com/locate/yjtbi

Stochastic simulation of actin dynamics reveals the role of annealing and fragmentation

Joseph Fass[a,b], Chi Pak[c], James Bamburg[c], Alex Mogilner[a,b,*]

[a]Department of Neurobiology, Physiology and Behavior, University of California, Davis, CA 95616-8633, USA
[b]Department of Mathematics, University of California, Davis, CA 95616-8633, USA
[c]Department of Biochemistry and Molecular Biology and Cell and Molecular Biology Graduate Program, Colorado State University

Received 6 November 2007; received in revised form 27 December 2007; accepted 7 January 2008
Available online 11 January 2008

Abstract

Recent observations of F-actin dynamics call for theoretical models to interpret and understand the quantitative data. A number of existing models rely on simplifications and do not take into account F-actin fragmentation and annealing. We use Gillespie's algorithm for stochastic simulations of the F-actin dynamics including fragmentation and annealing. The simulations vividly illustrate that fragmentation and annealing have little influence on the shape of the polymerization curve and on nucleotide profiles within filaments but drastically affect the F-actin length distribution, making it exponential. We find that recent surprising measurements of high length diffusivity at the critical concentration cannot be explained by fragmentation and annealing events unless both fragmentation rates and frequency of undetected fragmentation and annealing events are greater than previously thought. The simulations compare well with experimentally measured actin polymerization data and lend additional support to a number of existing theoretical models.

Keywords: Cytoskeleton; Monte Carlo simulations; Polymer length

1. Introduction

The dynamics of actin filaments are central to many cellular behaviors, including cell migration and cytokinesis (Bray, 2001). Classic experimental and theoretical studies during the 1970s and 1980s elucidated minute details of actin nucleation and the subsequent rapid elongation of actin filaments, and many relevant rates were measured directly and/or calculated (Oosawa and Asakura, 1975; Pollard, 1986; Wegner and Savko, 1982). Subsequently, the process of filament treadmilling—in which ATP-G-actin assembles at the growing barbed end, hydrolysis takes place in the middle of the filament, and ADP-G-actin dissociates from the shrinking pointed end—was predicted and observed (Pollard et al., 2000). It has also become clear that treadmilling alone does not explain all the observed actin turnover *in vivo*; rather, cells control the length distributions and dynamics of F-actin arrays via a host of actin accessory proteins such as ADF/cofilin, profilin, capping proteins, etc. (Pollard et al., 2000). Many experimental and theoretical studies have examined the effects of the various actin-binding proteins. However, many questions about basic, not modulated, actin dynamics remain unanswered. These include the nature and rates of γ-phosphate hydrolysis and release (Pieper and Wegner, 1996), the significance of different subunit conformations and orientations within the filament (Galkin et al., 2003), and the prevalence and nature of end-to-end filament annealing (Andrianantoandro et al., 2001; Howard, 2001), among others.

One of the relevant questions is about the character and nature of the changes of actin filaments' lengths in time. Recently, direct observations of actin filaments have become possible at timescales sufficient to address this issue. Convenient respective characteristic of F-actin dynamics is length diffusivity defined as the effective diffusion coefficient of a 'one-dimensional random walk'

*Corresponding author at: Department of Neurobiology, Physiology and Behavior, University of California, Davis, CA 95616-8633, USA. Tel.: +1 530 752 1072; fax: +1 530 752 6635.
E-mail address: mogilner@math.ucdavis.edu (A. Mogilner).

0022-5193/$ - see front matter © 2008 Elsevier Ltd. All rights reserved.
doi:10.1016/j.jtbi.2008.01.001

of a dynamic polymer in the length space: D is diffusivity if $\langle x^2 \rangle = 2\,Dt$, where x is the filament's length change, and t is the time, (Einstein, 1956). Thus, length diffusivity is calculated by plotting the mean squared length change—derived from a whole population of dynamic filaments—versus the time lag over which those changes are measured; for a diffusion-like process this produces a linear, increasing trend, and D is half the slope.

In the steady state, at the critical G-actin concentration, monomers assemble and disassemble from the filaments' ends with characteristic rate of the order of one monomer per second (Pollard, 1986; Pollard et al., 2000). Thus, expected length diffusivity for actin filaments at the critical concentration is $\sim$1 monomer^2/s. Two groups have recently used TIRF microscopy to observe the lengths of individual actin filaments (Fujiwara et al., 2002; Kuhn and Pollard, 2005), and in both cases observed, surprisingly, that the diffusivity $\sim$30 monomer^2/s was over an order of magnitude greater than that expected.

Various mechanisms have been proposed to explain this unexpected result: First, if a measurement error increases during the course of observation, this could effectively cause increasing artificial length changes and increasing calculated diffusivity. The statistics of the experimental errors are difficult to characterize, so at present this mechanism cannot be ruled out definitively; however, errors that are great enough to increase the diffusivity more than an order of magnitude are not very likely. One particular possible source of errors is pauses in filament length histories preventing subunit loss or addition that are either a natural yet heretofore unobserved behavior or arise from temporary attachments between filament ends and the glass coverslip. However, Fujiwara et al. (2002) did not observe pauses in filament length histories, while Kuhn and Pollard (2005) did but discarded obvious pauses in the analysis of the length diffusivity. Besides, the pauses would only increase the calculated length diffusivity for filaments undergoing net polymerization or depolymerization. Also, both groups calculated unexpectedly high length diffusivities at or near the critical concentration (Fujiwara et al., 2002; Kuhn and Pollard, 2005), where pauses should have little or no effect. Thus, undetected pauses are not likely to explain the length diffusivity observations.

Another explanation stems from possibility of the effective "dynamic instability"-like behavior similar to that observed in microtubules: rather than assembly and disassembly of single monomers, rescues and catastrophes may occur when a terminal ATP-actin subunit(s) is added or lost followed by rapid growth or shortening of the barbed end, respectively. Effectively, this would lead to longer and faster filament length excursions, and ultimately to a greater diffusivity. This mechanism has been addressed by two recent theoretical studies, both of which examined the dependence of length diffusivity on G-actin concentration (Vavylonis et al., 2005; Stukalin and Kolomeisky, 2006). By considering subunit addition and loss at barbed and pointed ends, and assuming random hydrolysis and slow phosphate release (consistent with rate constants in Pollard et al., 2000), Vavylonis et al. (2005) showed that the length diffusivity should reach the levels observed via TIRF microscopy ($\sim$30 monomer^2/s) just below the critical concentration, then drop to $\sim$1–5 monomer^2/s at and above the critical concentration. This behavior was attributed to mini-catastrophes/rescues, which are most prevalent just below the equilibrium concentration for ATP-actin at the barbed end. At such concentrations, "catastrophes" of consecutive ADP-actin losses and "rescues" of ATP-actin additions are both maximized. At concentrations very close to the critical concentration, however, treadmilling results in few ADP-actin subunits near the barbed end, and catastrophes decline.

Stukalin and Kolomeisky (2006) explored one more possible mechanism based on a vectorial, rather than random, ATP hydrolysis in the filaments. Their calculations showed that assuming a single vectorial hydrolysis and phosphate release step would result in high diffusivity ($\sim$30 monomer^2/s) just above the critical concentration. This is due to the fact that the vectorial hydrolysis "targets" ATP to ADP conversions to the barbed end, keeping the ATP cap small, which results in the effective "dynamic instability"-like behavior discussed above. However, they used a relatively large rate (0.3 s^{-1}) to describe the combined phenomena of vectorial hydrolysis and subsequent phosphate release. In addition, while still controversial experimental evidence favors random hydrolysis over vectorial or non-random mechanisms (Pieper and Weger, 1996).

Finally, there is a possibility that filaments' lengths fluctuate due to addition and loss of short fragments of F-actin, rather than individual monomers. These processes of annealing and fragmentation, respectively, would change filaments' lengths drastically and abruptly and could be the cause of the increased length diffusivity. There have been no detailed stochastic simulations of actin filaments' lengths that account for these processes. Therefore, we introduced these phenomena into stochastic simulations of populations of actin filaments to test the possibility that fragmentation and annealing complement subunit addition and loss to enhance length diffusivity. We found that at normal fragmentation rates the diffusivity at critical concentrations remained low, and only a combination of enhanced fragmentation rates and experimental errors greater than expected could increase the diffusivity to the observed level.

We also used the simulations to examine the effects of filament annealing and fragmentation on the nucleotide distribution within the filaments, polymerization kinetics and filament length distribution. Both the polymerization kinetics and nucleotide profiles were largely unaffected by the incorporation of annealing and fragmentation. The filament length distribution, on the other hand, changed drastically, from broad, flat and initial condition dependent in the absence of annealing and fragmentation to a stable stationary exponential distribution (independent of initial

conditions) in their presence, in agreement with previous experimental studies (Kas et al., 1996; Sept et al., 1999). Finally, our simulations support a number of existing simplified models of actin dynamics.

2. Methods

The list of the modeled processes can be found in the Supplemental Material. Monte Carlo simulations were performed using Gillespie's First Reaction algorithm (Gillespie, 1977; Gibson and Bruck, 2000). A random time interval was generated for each possible event in the reaction volume V: nucleation (subunit addition to a trimer); complete depolymerization of a filament (loss of a subunit from a tetramer); ATP-actin addition to a filament's barbed or pointed end; ATP-, ADP · P_i-, or ADP-actin loss from a barbed or pointed end; γ-phosphate hydrolysis; γ-phosphate release; filament–filament annealing; random fragmentation; stress-induced fragmentation (Fig. 1). Actin dimer concentration was calculated assuming equilibrium with monomers, and then trimer concentration was calculated assuming equilibrium with dimers. Rate constants from Brownian dynamic simulations were used for both calculations (Sept and McCammon, 2001). Table 1 shows the values and references for all the rate constants used. All events were modeled as first-order or pseudo-first-order events, and time intervals generated according to the equation $t = -\ln(r)/k$, where r is a uniformly distributed random number on (0,1), and k is the first-order or effective pseudo-first-order rate constant. For N independent, identical events with the same rate constant k', the effective rate constant $k = Nk'$ was used. After the time intervals for all possible events were generated, the event with the minimum time interval was then implemented, the current time of the simulation was updated by that time step, and then the whole process was repeated.

In order to save the calculation time, we only generated one random time interval for annealing at each time step: $t = -\ln(r)/(Nk_a)$, where k_a has units of seconds^{-1} and is the pseudo-first-order annealing rate constant of the form $k_a = [N](10\,\mathrm{s}^{-1})/(1 + 0.01\langle L\rangle)$, where $[N]$ is the number concentration of filaments and $\langle L\rangle$ is the mean filament length in subunits. This form for k_a was suggested by Andrianantoandro et al. (2001). If the annealing time was the minimum time, we then chose a random barbed end and a random pointed end to anneal. Using this method for simulation of annealing, we were able to reproduce the experimental results of Andrianantoandro et al. (2001) with very little error (Supplemental Fig. S1).

We simulated two pathways for fragmentation using the random and stress-induced mechanisms described in Sept et al. (1999). For random fragmentation, a random time was generated for each filament using the rate constant $k_i = k_{fr}L_i$. For stress-induced fragmentation, a random time was generated for each filament using $k_i = k_{fs}\langle L\rangle^2[N]$; k_{fr} and k_{fs} are listed for random and stress-induced fragmentation in Table 1. If either fragmentation mechanism had the minimum event time, a random site for fragmentation was chosen, with no biases, from every subunit–subunit bond in the appropriate filament.

The state (ATP-, ADP · P_i-, ADP-actin) and relative position of each subunit within each filament in the simulation volume was tracked. The positions and orientations of filaments within the volume were not simulated. Because the model was not spatial in nature and filaments within the simulation volume were taken to be representative of an arbitrarily larger reaction volume, diffusive movement of filaments into and out of

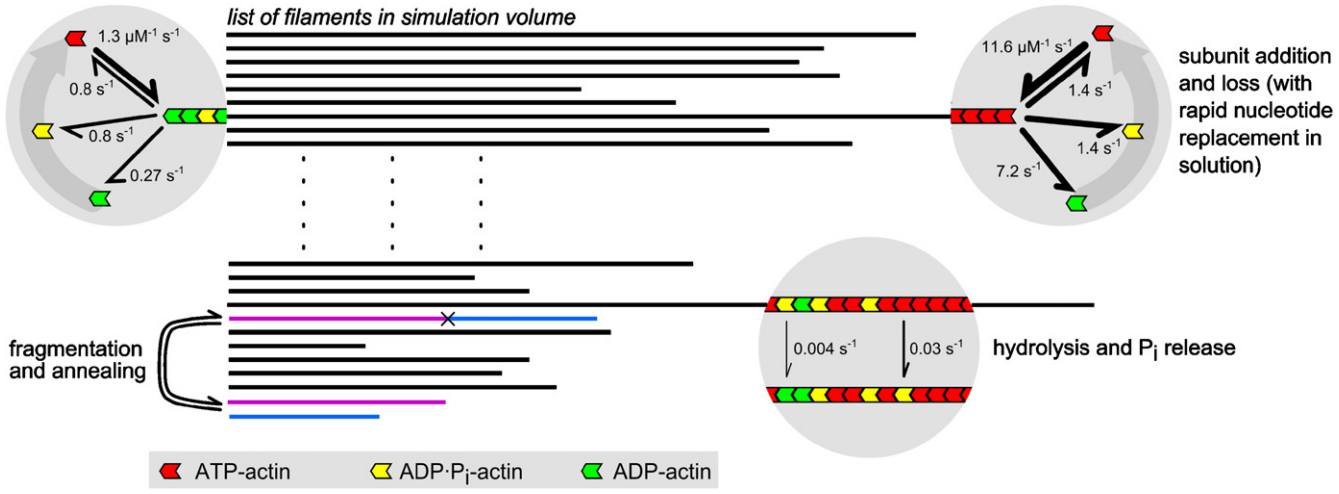

Fig. 1. Elements of the model: subunit addition and loss from the fast-growing barbed end (to the right) and slow-growing pointed end (to the left) are modeled, as well as random phosphate hydrolysis and release within each filament. Nucleotide replacement (ATP for ADP or ADP · P_i) is assumed to occur instantaneously once a subunit is in solution. In addition, we model two mechanisms of filament fragmentation (random and stress-induced) as well as end-to-end annealing (see text) (constants for all reactions are listed in Table 1).

Table 1
Rate constants used in simulations

Event	Rate Constant	Reference
Nucleation steps		
Monomer to dimer	$35.7\,\mu M^{-1}\,s^{-1}$	Sept and McCammon, 2001
Dimer to monomer	$1.63e8\,s^{-1}$	Sept and McCammon, 2001
Dimer to trimer	$2.18\,\mu M^{-1}\,s^{-1}$	Sept and McCammon, 2001
Trimer to dimmer	$1.3e3\,s^{-1}$	Sept and McCammon, 2001
Subunit addition/loss		
ATP-actin addition at barbed end	$11.6\,\mu M^{-1}\,s^{-1}$	Pollard, 1986
ATP-actin addition at pointed end	$1.3\,\mu M^{-1}\,s^{-1}$	Pollard, 1986
ATP-actin loss from barbed end	$1.4\,s^{-1}$	Pollard, 1986
ADP · P_i-actin loss from barbed end	$1.4\,s^{-1}$	Pollard, 1986
ADP-actin loss from barbed end	$7.2\,s^{-1}$	Pollard, 1986
ATP-actin loss from pointed end	$0.8\,s^{-1}$	Pollard, 1986
ADP · P_i-actin loss from pointed end	$0.8\,s^{-1}$	Pollard, 1986
ADP-actin loss from pointed end	$0.27\,s^{-1}$	Pollard, 1986
Hydrolysis (ATP-to ADP · P_i-actin)	$0.3\,s^{-1}$	Blanchoin and Pollard, 2002
Phosphate release (ADP · P_i-to ADP-actin)	$0.004\,s^{-1}$	Vavylonis et al., 2005
Fragmentation/Annealing		
Random fragmentation	$1.1e\text{-}8$ subunits$^{-1}\,s^{-1}$	Sept et al., 1999
Stress-induced fragmentation	$1.8e\text{-}8$ subunits$^{-2}\,\mu M^{-1}\,s^{-1}$	Sept et al., 1999
Annealing	$[10/(1+0.01\times\langle L\rangle)]\,\mu M^{-1}\,s^{-1}$	Andrianantoandro et al., 2001

the volume were not considered. The size of the simulation volume was adjusted in order to keep the number of filaments within a chosen range (usually 300–600) as follows. If, due to nucleation or fragmentation events, the number of filaments increased beyond the chosen upper limit, the size of the simulation volume was decreased by one-third, and each filament was given a 1 in 3 chance of being discarded. If, due to depolymerization or annealing, the number of filaments decreased beyond the chosen lower limit, the size of the simulation volume was increased by 50% and each filament was given a 1 in 2 chance of being duplicated and the duplicate then, added to the list of filaments within the simulation volume. This alleviated the dilemma between choosing a large fixed simulation volume, which would allow initial nucleation over a reasonable timescale but cause very slow computation once many filaments had formed, and a small fixed simulation volume, which would run quickly later on at high filament number concentrations, but in which nucleation would be poorly modeled as only one filament would represent the whole reaction volume at early times.

In order to simulate the experimental conditions in Fujiwara et al. (2002) we chose to start with a higher initial concentration of free actin than the 0.3 μM they used (for Mg-actin), because in simulations 0.3 μM actin requires on the order of 24 h to fully polymerize. This is due, most likely, to the presence of small numbers of proteins that modulate actin dynamics in experimental purifications. Instead, we started simulations at 3.0 μM, then after 5 min reset the concentration to 0.3 μM, and allowed it to change freely after that. This resulted in a rapid initial burst of nucleation which allowed the simulated concentration to reach the critical concentration (~0.14 μM) in about an hour, much closer to the reported time of ~20–25 min (Fujiwara et al., 2002).

Measurements were simulated by recording the lengths of all the filaments in the simulation volume at one-minute intervals after the critical concentration was attained. However, in order to adequately simulate the measurement process employed by Fujiwara et al. (2002) and Kuhn and Pollard (2005), we needed to discard length histories in which obvious annealing events took place, as both groups did. In addition, neither group observed fragmentation. This may have been because all filaments under observation were attached at one or several points to the glass coverslip, which may have stabilized them against fragmentation. Nevertheless, short segments at the ends of filaments could still have undergone fragmentation while escaping detection via time-lapse imaging. In order to account for both of these experimental phenomena, we used a parameter henceforth referred to as the "detectability limit" in our analysis of filament length histories. The detectability limit represents a threshold length change such that either (i) an observer would have discarded the length history (in the case of annealing events), or (ii) the event would have been prevented by coverslip attachment (in the case of fragmentation events). While the length limits on these two phenomena could differ, we chose to introduce only one free length threshold parameter to our model.

Rather than discard all the measurements in a length history, we simply broke a length history into two consecutive histories if an instantaneous (i.e. from one event to the next) length change greater than the detectability limit occurred. However, two consecutive measurements could still differ by an amount greater than the detectability limit due to several individual changes that are each less than the detectability limit, in addition to the contribution of subunit addition or loss. In addition, zero-mean Gaussian measurement error with a standard deviation of 0.54 μm, consistent with the error reported by Fujiwara et al. (2002), was added to all recorded lengths, increasing the possibility that two consecutive measurements could differ by more than the detectability limit.

3. Results

3.1. Simulations of filament populations reveal minute details of actin dynamics

Variable volume stochastic simulations of actin polymerization allow vivid illustration of the evolution of filament length distributions during polymerization. Fig. 2 shows the polymerization kinetics (Fig. 2A) and the average filament lengths (Fig. 2B) over 24 h for different initial free actin concentrations. Polymerization kinetics at given rates of actin dynamics is insensitive to the presence or absence of normal fragmentation/annealing. It is characterized by, first, an initial lag phase which can last for several hours for initial G-actin concentrations below 1 μM and is a decreasing function of this concentration. The amount of F-actin then increases linearly over a period of hours until saturation, at which G-actin reaches the critical concentration: ~0.14 μM. At actin concentrations in the range of 1–10 μM, the lag and growth phases decrease to minutes. The simulated features of the polymerization kinetics in the absence of the fragmentation/annealing are in qualitative agreement with earlier data and calculations (Cooper et al., 1983; Tobacman and Korn, 1983).

Although polymerization curves produced by simulations with and without fragmentation and annealing are similar, the evolution of filament length distributions is quite different. Initially, prior to the significant G-actin depletion, the nucleation and filament elongation rates are almost constant, so the filaments appear and grow at constant rates resulting in roughly uniform length distribution, the upper limit of which grows linearly with time. Then, as G-actin is depleted, the nucleation rate, which is a high power of the G-actin concentration, drops rapidly. In the absence of fragmentation and annealing, the filaments continue to elongate for a while until the G-actin concentration decreases to the critical concentration, at which the length distribution evolves into a wide and irregular peak (Fig. 3) dependent on the initial conditions and with an average length on the order of tens of microns, in qualitative agreement with the experimental data (Kas et al., 1996).

When fragmentation and annealing are accounted for, however, the evolution of the filament length distribution is markedly different. Fragmentation produces filament ends rapidly after very little nucleation and growth has occurred. This in turn depletes the G-actin concentration much more rapidly. Thus, the slowing of nucleation occurs almost simultaneously with the onset of significant fragmentation, after which the fragmentation rates increase to fairly constant levels. Annealing event rates increase as the number concentration of filaments increases. This progression depends on the initial free actin concentration, and is more rapid at higher concentrations. Fragmentation reduces the number of long filaments resulting first in a Poisson-like length distribution, and then, as the G-actin concentration reaches the critical concentration, in a stationary exponential distribution (Fig. 3), in which the

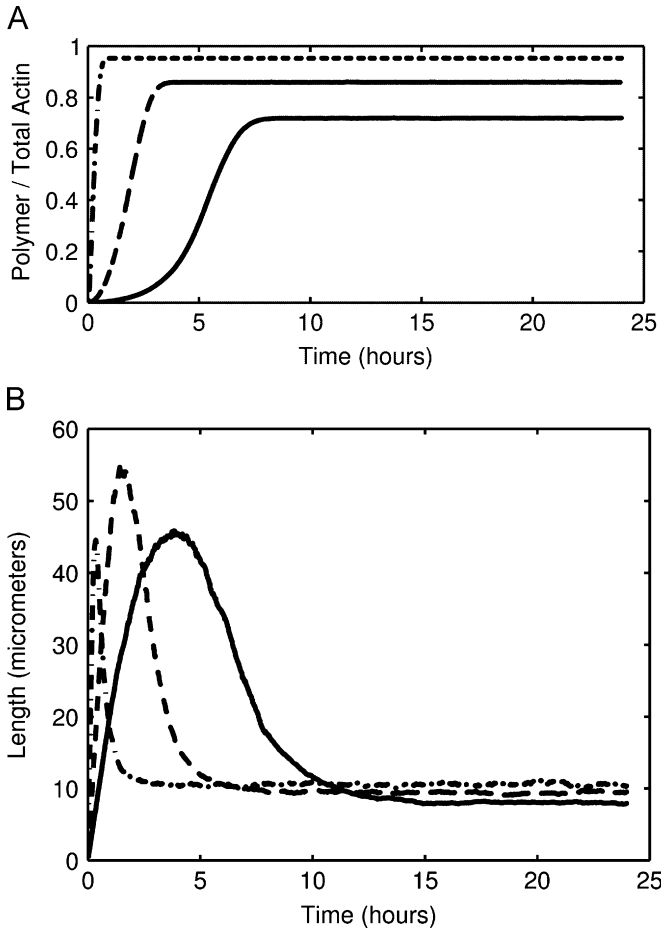

Fig. 2. Polymerization kinetics. F-actin as a function of time resulting from simulations with 150–300 filaments is shown for total actin concentrations of 0.5 (*solid*), 1.0 (*dashed*), and 3.0 μM (*dash-dot*). Data are averaged from 5 simulations at each concentration. (A) Time series for polymerized fraction for all three total actin concentrations. (B) Average lengths for simulated populations, corresponding to simulations in (A).

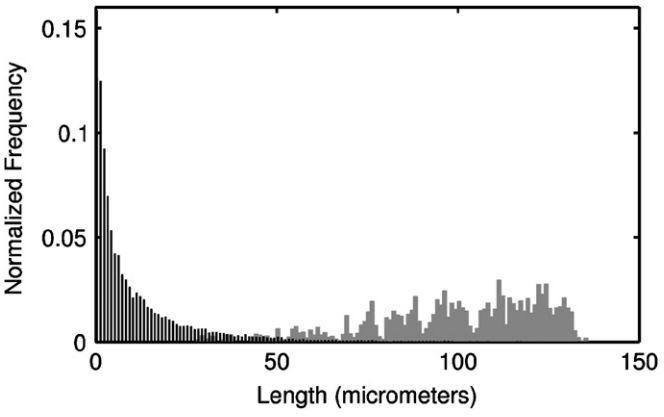

Fig. 3. Steady state length distributions: Length distributions at steady state (~15–24 h) are shown for simulations with 3.0 μM total actin both with and without normal annealing and fragmentation (*black bars* and *gray bars*, respectively). Distributions were averaged from 50 time points taken at 10 min intervals from ~15–24 h.

average filament length is determined by the balance of fragmentation and annealing and is ~10 μm (Fig. 2B), in qualitative agreement with earlier experiments and approximate calculations (Oosawa and Asakura, 1975; Sept et al., 1999).

3.2. Higher fragmentation rates result in faster polymerization kinetics

Recent experimental approaches used labeled actin monomers to visualize filaments (Fujiwara et al., 2002; Kuhn and Pollard, 2005), so there may have been an abnormal level of fragmentation in these studies. Indeed, neither the TMR- nor the OG-actin used in these studies can polymerize unless there are unlabeled G-actin monomers present with which they can copolymerize (Kuhn and Pollard, 2005; Kudryashov et al., 2004). TMR-actin and unlabeled actin copolymers have been reported to polymerize faster than pure unlabeled actin, and copolymerization results in shorter filaments (Kudryashov et al., 2004), both presumably due to increased fragmentation of F-actin. In order to simulate the presence of TMR- or OG-actin, we ran simulations in which the random fragmentation rate constant was increased by factors of 5, 10, 50, 100, and 200, with an initial free actin concentration of 6 μM (to facilitate comparison to the results of Kudryashov et al. (2004). The resulting polymerization time series (Fig. 4) show that increasing the fragmentation rate advances the polymerization curve and increases the greatest observed polymerization rate. We used these simulations to roughly calibrate against the experimental observations in Kudryashov et al., 2004, where ~8 and ~17% TMR-actin polymerization were advanced with respect to that of pure unlabeled actin (Fig. 4, inset) to roughly the same degree as simulated actin with 50-, 100-, or 200-fold increased random fragmentation. Note that TMR-labeled actin was also observed to delay the initial nucleation phase by several minutes, suggesting that TMR-actin also affects nucleation (Marques et al., 1994). We did not attempt to reproduce this effect of copolymerization.

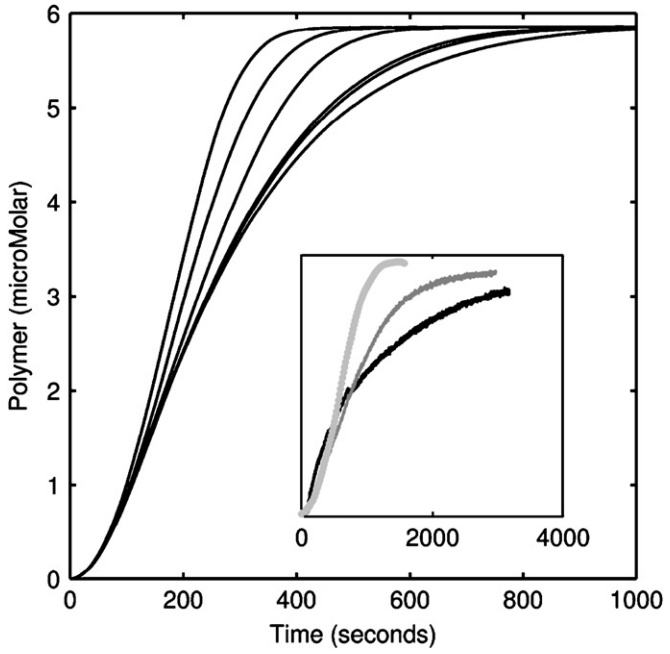

Fig. 4. Simulated polymerization curves for various fragmentation rates. Initial concentration for all the simulations is 6 μM. Curves show polymerized actin for simulations in which the random fragmentation rate constant was multiplied by a factor of (from right to left) 1 ×, 5 ×, 10 ×, 50 ×, 100 ×, and 200 ×. *Inset*: Experimental polymerization curves for pure actin (*black*), 1:12 TMR-actin to unlabeled actin (8.3% labeled; *dark gray*), and 1:6 TMR- to unlabeled actin (16.6%; *light gray*). Horizontal axis is seconds, vertical axis is absorbance. Raw data for inset provided by Dmitri Kudryashov.

3.3. Fragmentation and annealing events affect neither nucleotide profiles within filaments, nor barbed ends length excursions

The recently observed high F-actin length diffusivities (Fujiwara et al., 2002; Kuhn and Pollard, 2005) could originate from length changes resulting directly from more frequent fragmentation and annealing events, or indirectly due to increased fragmentation exposing ADP-actin subunits (normally protected by the ATP-actin cap) allowing mini-catastrophes and rescues of filament ends. In order to investigate the causes of the observed F-actin dynamics, we looked at the composition of the barbed-end terminal subunit(s) under various simulated conditions. First, we explored the dependence of the state of the barbed end-terminal subunit on free actin concentration, by analyzing data from simulations in which constant concentrations ranging from 0.03 to 3.0 μM were imposed after a simulation reached the critical concentration. The fraction of terminal subunits in each state did not depend upon the presence of annealing and fragmentation, or a 50-fold increased fragmentation rate (Fig. 5A). The exposure of ADP-actin at the first subunit is high at sub-critical concentrations, but decreases to almost zero at the critical concentration and above; at a concentration of 0.14 μM the barbed-end terminal subunit was ATP-actin 69.1% of the time, ADP · P_i-actin 30.4% of the time, and ADP-actin 0.5% of the time, for simulations with 3.0 μM total actin.

Next, we looked at the composition of the first micrometer (370 subunits) at the barbed end during a period of 30 min after the critical concentration was reached (Fig. 5B). In each of three cases (no annealing or fragmentation, normal fragmentation and annealing, and 50-fold increased fragmentation rate with normal annealing), the fractions of ATP-, ATP · P_i-, and ADP-actin at each position are plotted. The results show that the steady-state nucleotide profiles of the first micrometer within filaments, as well as the state of the barbed end-terminal subunit, are unaffected by fragmentation and annealing. These profiles agree roughly with those predicted by Binschadler et al. (Fig. 3A, B in Bindschadler et al. (2004); note that their parameter set is different than ours)

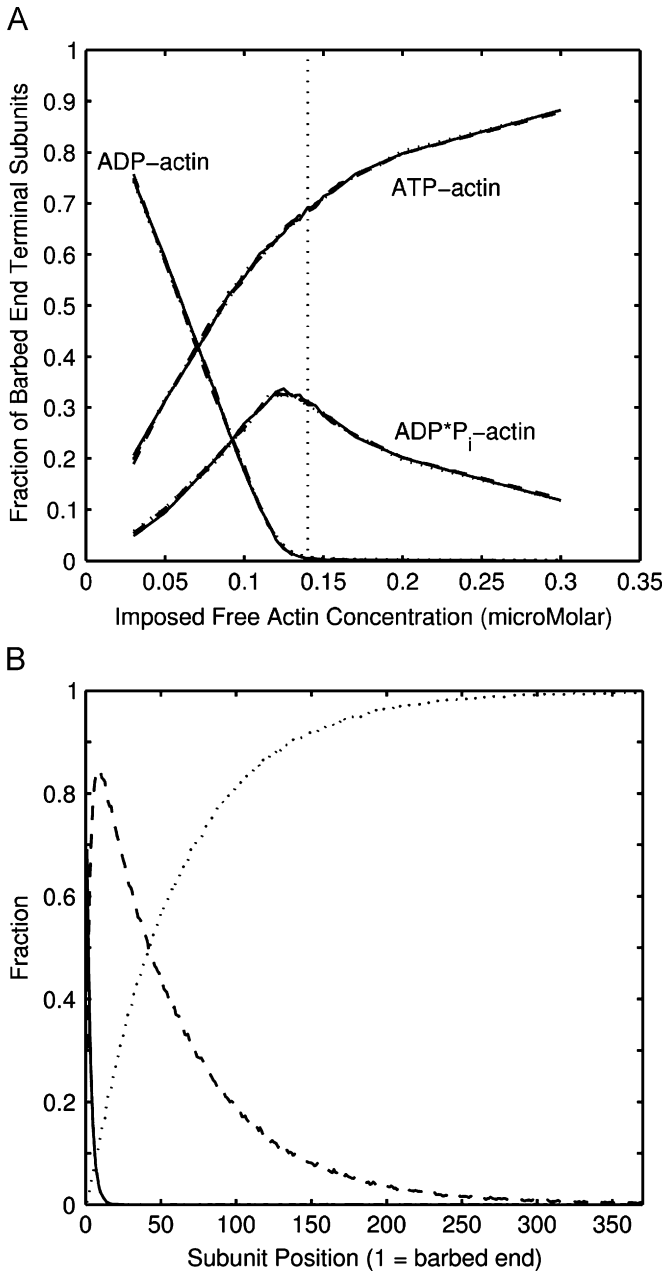

Fig. 5. Nucleotide states of simulated actin filaments. (A) State of barbed-end terminal subunit versus imposed free actin concentration, at steady state. Curves are shown for 5 simulations: one with no annealing or fragmentation (*solid line*), two with normal annealing and fragmentation (*dashed lines*), and two with 50 × increased fragmentation rates (*dotted lines*). Vertical line (*dash-dot*) indicates critical concentration (0.14 μM). (B) States of the first 370 barbed-end terminal subunits at steady state, for 3.0 μM total actin. The fraction of subunits at each position, averaged across all filaments in the simulation volume, in each nucleotide state is shown: ATP- (*solid*), ADP · P_i- (*dashed*), and ADP-actin (*dotted*).

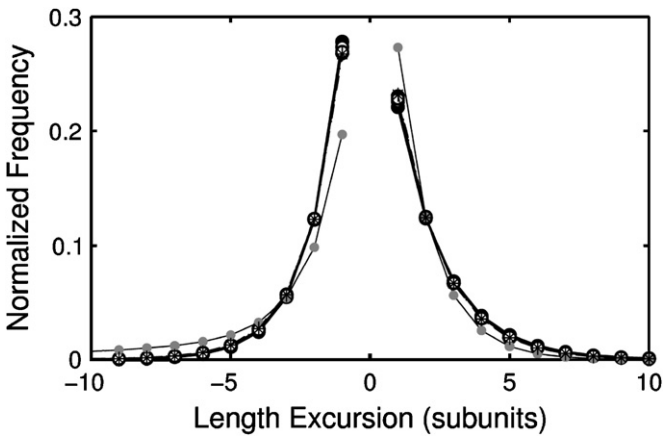

Fig. 6. Lengths of excursions (repeated loss or gain of subunits) at the barbed ends of filaments. Excursions were measured by tracking the lengths of repeated loss or gain of subunits that were then terminated by subunit gain or loss, respectively. Excursions terminated by annealing or complete depolymerization events were not included in this analysis. Measurements were made during the period of 4000–5800 s, from simulations of 3.0 μM total actin, beginning when the free actin concentration was close to the critical concentration (for the no fragmentation or annealing case) or had reached the critical concentration (all other cases). Curves are shown for no fragmentation or annealing (*solid, filled circles*) and 1 ×, 10 ×, 50 ×, 100 ×, and 200 × fragmentation rates with normal annealing (*solid/open circles*, *dashed/closed*, *dashed/open*, *dotted/closed*, *dotted/open*, respectively) from simulations in which no concentration was imposed. The maximum variation among these curves is for excursions of length −1 (3.6%) and +1 (4.1%). Also shown are two curves from simulations with normal annealing and fragmentation in which concentrations of 0.10 (*solid line, small gray circles*) and 0.14 μM (*dashed line, asterisks*) were imposed starting at 3600 s. In the simulations, the most frequent barbed-end excursion lengths for imposed concentrations of 0.10 and 0.14 μM were from 1 to 4 subunits, and the most frequent excursion durations were between 0.6 and 0.9 s. Excursions at the pointed end were roughly the same magnitude, but slower (longer duration).

lending further support to the approximate model in Bindschadler et al. (2004).

Finally, we investigated length excursions of the barbed ends by tracking the persistence of subunit losses or gains. Only excursions that ended with a reversal, i.e. subunit addition (loss) event after a loss (gain) of a few subunits, were counted; excursions ended by an annealing or complete depolymerization event were discarded. The distribution of length excursions during a period of 30 min after the critical concentration was reached is shown for various fragmentation rates (Fig. 6). The distribution shows that the excursion lengths are distributed exponentially, as is the 'memory-less' dynamic instability phenomenon described in microtubules, but on the average are only a few subunits long, unlike the dynamic instability. The difference between the distributions corresponding to simulations without fragmentation and annealing and various fold-increases in the normal fragmentation rate (up to 200-fold) is very small: the greatest difference, for the frequency of 1 subunit addition/loss, is ~4%. The results illustrated in Figs. 5 and 6 suggest that the addition and loss dynamics at the ends of filaments is not greatly altered by the inclusion of normal or even enhanced fragmentation and annealing in simulations.

3.4. Simulations yield high diffusivities only if large length changes and higher fragmentation rates are allowed

In order to calculate length diffusivity in a manner similar to the one used in Fujiwara et al. (2002), we

examined simulated length histories in a 30 min interval soon after the critical concentration was reached (~1 h after simulations were begun). We processed simulation results using a range of detectability limits from 0.5 μm (close to the measurement error) to 2 μm. This limit was, in our opinion, a maximum believable annealing or fragmentation event that could be missed by an experimenter between image acquisitions. Higher detectability limits resulted in higher calculated diffusivities (Fig. 7). This is to be expected, because analysis of the same length histories with higher detectability limits means that fewer large annealing and fragmentation events are excluded from the calculation of length diffusivity.

When no annealing or fragmentation was allowed, or at normal level of annealing and fragmentation, the detectability limit had almost no effect on low length diffusivity (Fig. 7). Thus, normal levels of annealing and fragmentation would not likely account for the high length diffusivities observed experimentally. As argued above, 50- to 200-fold fragmentation rate increases possibly accompanied TMR- or OG-actin assembly in the experiments, so we calculated diffusivities from simulated length histories with increased fragmentation rates (Fig. 7). High fragmentation rates did not greatly affect the calculated diffusivity at a detectability limit of 0.5 μm, but had large effects at higher detectability limits. The simulations, even at very high detectability limit of 2 μm, cannot explain measured diffusivities above 30 monomers^2/s at normal, or ten-fold increased fragmentation rates. The minimum detectability limit which would have to be assumed in order to obtain measured diffusivities above 30 monomers^2/s decreases with increasing fragmentation rate is ~1.5 μm for 50 × fragmentation, and ~1 μm for 100 × fragmentation. Thus, only rates of fragmentation increased two orders of magnitude (consistent with the fractions of labeled actin monomers used in both experimental studies) could have led to the high length diffusivities, if it is assumed that experimenters could have missed fragmentation or annealing events on the order of ~1–1.5 μm. We find this very believable because such fragments could appear in or disappear from the plane of focus quite easily between image acquisitions, and the resulting length changes would have been masked by measurement error on the order of 0.5 μm.

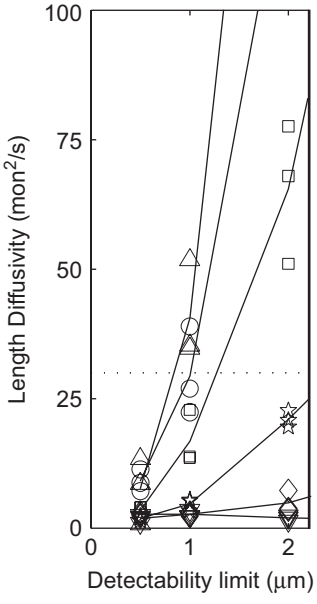

Fig. 7. Length diffusivities calculated from simulations at various random fragmentation rates (no fragmentation or annealing, downwards pointing triangles; normal fragmentation and annealing, diamonds; and normal annealing with increased random fragmentation: 10 ×, *stars*; 50 ×, *squares*; 100 ×, circles; 200 ×, *upwards pointing triangles*), analyzed using detectability limits (see text) from 0.5 to 2 μm. Data from three runs for each parameter set are shown (*open symbols*), along with average (*solid lines*).

3.5. Length diffusivity dependence on actin concentration

Because Fujiwara et al. used 10% TMR-actin in their studies (Andrianantoandro et al., 2001), we chose to focus on a 50-fold increase in fragmentation as most representative of the experimental conditions (Fig. 4). We analyzed the dependence of diffusivity on detectability limit and fragmentation (no fragmentation or annealing, normal fragmentation and annealing, and 50-fold increased random fragmentation rate with normal annealing) at imposed concentrations from 0.03 to 0.3 μM (Fig. 8). With no fragmentation or annealing, there is no dependence on the detectability limit, and diffusivity reaches a peak of 30–40 monomers^2/s at around 0.1 μM, and drops back to 1–5 monomers^2/s at and above the critical concentration (Fig. 8A). This result is in good agreement with the conclusions of Vavylonis et al. (2005). At normal fragmentation and annealing rates, and 50-fold increased fragmentation rates, diffusivities increase with increasing detectability limits, but largely keep the same dependence on concentration (Fig. 8B, C).

4. Discussion

Impressive recent gains in quantitative understanding of actin dynamics are due in no small measure to modeling efforts accompanying experimental studies (Pollard and Borisy, 2003). The most popular approach to modeling is to describe actin populations using differential equations (Oosawa and Asakura, 1975; Sept et al., 1999; Bindschadler et al., 2004; Ermentrout and Edelstein-Keshet, 1998). Recently, this approach allowed the prediction of spatial distributions of the nucleotide profiles within filaments (Bindschadler et al., 2004). Earlier, solutions of differential equations describing polymerization and gelsolin-induced fragmentation, but not annealing (Ermentrout and Edelstein-Keshet, 1998), predicted transient peaks in filament length distributions and monotonically decreasing stationary length distributions. There is also rich literature on fragmentation/annealing modeling in non-actin systems (VanDongen and Ernst, 1984; Marques et al., 1994), in

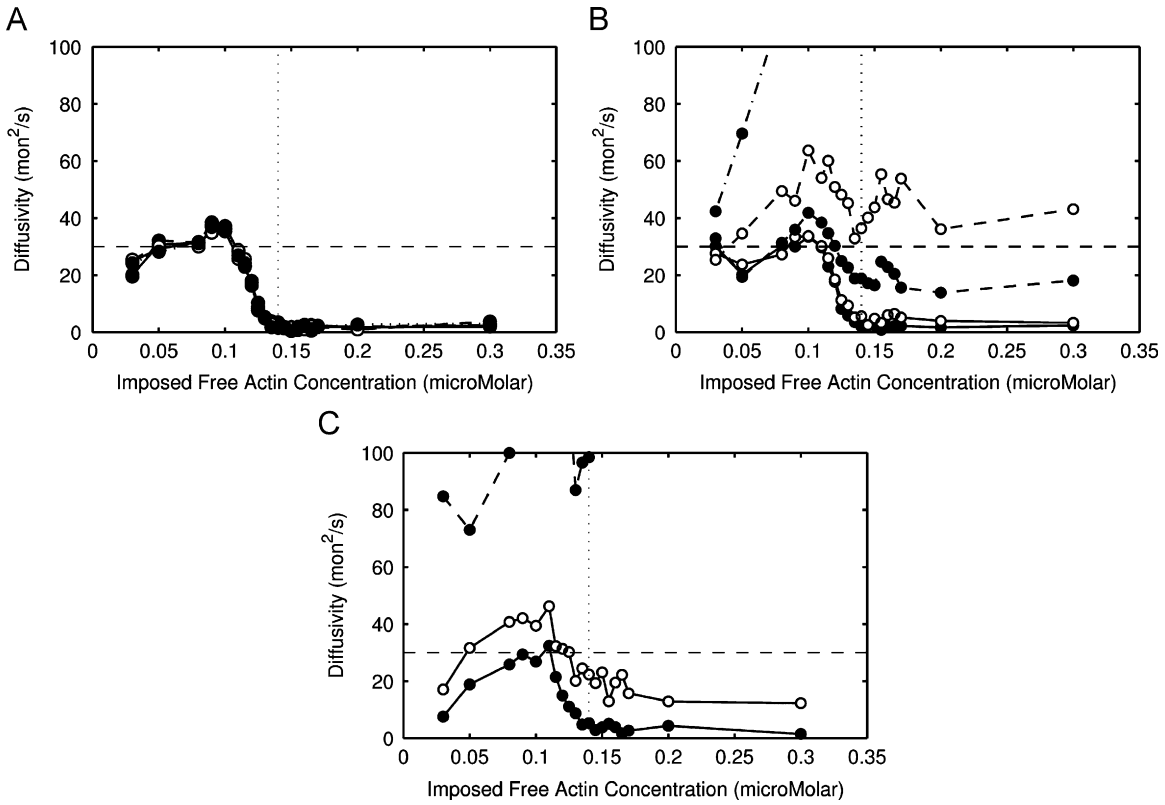

Fig. 8. Diffusivity versus free actin concentration for 300–600 filament simulations with (A) no annealing or fragmentation, (B) normal annealing and fragmentation, and (C) 50-fold increased fragmentation rate with normal annealing. Curves are plotted for detectability limits of 0.5 μm (*solid, filled circles*), 1.0 μm (*solid, open circles*), 2.0 μm (*dashed, filled circles*).

which both stationary polymer size distributions and temporal transients leading to these distributions were investigated. These efforts were forced to use approximations, and could only follow a finite number of descriptors of a population (e.g. mean and standard deviation of filament lengths). The danger of these approximations is that small changes in the model assumptions can have drastic consequences for the model results (Ermentrout and Edelstein-Keshet, 1998). Stochastic simulations (one of the first such efforts were Monte Carlo-type simulations VanDongen and Ernst, 1984), on the other hand, can explicitly follow each filament and subunit in a population, but efforts in this area to date have excluded the important processes of fragmentation and annealing (Vavylonis et al., 2005; Dufort and Lumsden, 1993) with the exception of several studies of the combined effects of severing, capping and branching on the critical concentration of actin (Carlsson, 2005, 2006).

In this study, we used Gillespie's stochastic simulation algorithm in order to simulate F-actin dynamics, including the processes of fragmentation and annealing (Gillespie, 1977). We implemented recent models of fragmentation (Sept et al., 1999) and annealing (Andrianantoandro et al., 2001), which allowed rapid simulation of *in vitro* polymerization of purified actin. Nevertheless, several simplifying assumptions were made in order to yield reasonable computation times. The first of these was the assumption that ATP replaces ADP on G-actin instantaneously; i.e. there is no ADP-G-actin. We were able to run simulations without this simplification, and found that although it affected the critical concentration somewhat, other aspects of filament dynamics and composition were almost completely unaffected (Supplemental Fig. S2). The second simplification was using average filament length to calculate fragmentation (random and stress induced) and annealing times. A more realistic approach might be to calculate separate times for each filament (for fragmentation) and pair of filaments (for annealing) based on their individual lengths (Hill, 1983). However, our model was able to closely reproduce data from experiments in which annealing and fragmentation were ostensibly the only events that could occur (Supplemental Fig. S1). Since there is no direct empirical data correlating the annealing or fragmentation of individual filaments to their lengths, we feel that our approach is as accurate as possible at this time. Nevertheless, future simulations that do not employ this simplification may be revealing.

Our results for polymerization kinetics in the absence of fragmentation/annealing are in a very good qualitative agreement with earlier data and calculations (Cooper et al., 1983; Tobacman and Korn, 1983). We predict that at low

fragmentation rates the polymerization kinetics is not affected by fragmentation/annealing. However, at higher fragmentation rates, the polymerization curve is characterized by a more abrupt transition between the growth phase and saturation, in qualitative agreement with earlier studies (Wegner and Savko, 1982; Frieden and Goddette, 1983). Similarly, we observed that fragmentation and annealing have little influence on the nucleotide profiles within filaments, which are similar to those predicted by a previous model (Bindschadler et al., 2004) that used significant simplifications.

Without fragmentation and annealing, our simulations predict a broad and irregular distribution of filament lengths with an average length of tens of microns, which is in qualitative agreement with the experimental data (Kas et al., 1996; Limozin et al., 2003). Early evolution of the filaments' length distribution derived from our simulations agrees qualitatively with theoretical conclusions of Hu et al. (2006): after early nucleation and initial elongation phases, the length distribution undergoes effective 'diffusive' redistribution of subunits between the filaments for a few hours. The addition of annealing and fragmenting causes a drastic change in the F-actin length distribution, making it exponential, in agreement with earlier data and approximate calculations (Sept et al., 1999). The reason for the exponential distribution at steady state is the balance between the fragmentation of longer filaments and annealing of shorter ones, resulting in a characteristic mean length that is largely independent of the monomer concentration. Our simulations predict a mean length of $\sim$10 μm that is very close to experimental observations (Sept et al., 1999).

One of the motivations for this work was recent observation of high length diffusivities by Fujiwara et al. (2002) and Kuhn and Pollard, (2005) surprising because it suggested that accepted mechanisms of F-actin dynamics are incomplete. Our results indicate that some combinations of high fragmentation rates (i.e. 50-fold higher or more, which is plausibly a consequence of the use of labeled actin) and high detectability limits (i.e. 1–1.5 μm, which is plausibly due to the limits of resolution and the lack of continuous image capture) may explain high observed F-actin length diffusivity. The simulations show that these recent observations are not inconsistent with random hydrolysis and phosphate release and may be a direct result of annealing and fragmentation of short fragments, rather than enhanced exposure of ADP-actin in filaments.

The remaining issue, however, is why such high fragmentation rates were not observed directly in the experiments on length diffusivity, and how likely high detectability limits are. It is also not clear how likely are the simultaneous occurrence and congruence of high fragmentation rates and high detectability limits. Our simulations merely indicate quantitatively the conditions under which the experimental results could be explained by the combination of experimental error, fragmentation and annealing. If these conditions are not met, the search for the explanation would have to expand.

Further complexities in actin dynamics may also affect length diffusivity. For example, some evidence suggests that actin subunits undergo conformational changes over a period of minutes to hours following polymerization that increase the local stability of the filament (Orlova et al., 2004). Such stabilization would bias fragmentation events towards the barbed end in polymerizing or treadmilling populations, thereby increasing the frequency of short (e.g. <1 μm) length changes, which could also account for some portion of high observed length diffusivities. This example illustrates the utility of combining modeling and experimentation approaches, as future studies could predict the degree to which standard models of actin dynamics might be inaccurate, as the experimental data to both suggest and verify inaccuracies becomes available.

In the future, modeling will also have to address possible roles of the fragmentation and annealing in cell migration and other *in vivo* processes. One of the relevant puzzles is the appearance of the 'brushwork' of short filaments at the leading edge of the lamellipodia followed by a more regular network of apparently longer filaments, as gleaned from the EM images (Pollard and Borisy, 2003). One possible scenario that could explain this structure is uncapping of the filament pointed ends (detachment of Arp2/3) followed by annealing of the uncapped pointed ends with the growing barbed ends. Also, predicted filament length distributions could have important implications for length-sensitive mechanical properties of the actin cortex underlying biophysics of cell movements (Bray, 2001; Howard, 2001). Transient changes in filaments' length and chemical state could be caused by rapid changes in the fragmentation and annealing kinetics and affect rapid changes in cell motile states. Modeling of these scenarios will require explicit stochastic simulations of the actin networks in space and time, taking into account specific reactions with actin binding proteins affecting the fragmentation and annealing rates.

Acknowledgments

This work was supported by the National Science Foundation Grant DMS-0715729 to A.M. and Predoctoral Fellowship DGE-0234615 to C.P., and by National Institutes of Health Grants NS43115 to J.F., GM35126 and NS40371 to J.B., and GLUE Grant "Cell Migration Consortium" (NIGMS U54 GM64346) to A.M.

Appendix A. Supplementary materials

The online version of this article contains additional supplementary data. Please visit doi:10.1016/j.jtbi.2008.01.001.

References

Andrianantoandro, E., Blanchoin, L., Sept, D., McCammon, J.A., Pollard, T.D., 2001. Kinetic mechanism of end-to-end annealing of actin filaments. J. Mol. Biol. 312, 721–730.

Bindschadler, M., Osborn, E.A., Dewey Jr, C.F., McGrath, J.L., 2004. A mechanistic model of the actin cycle. Biophys. J. 86, 2720–2739.

Blanchoin, L., Pollard, T.D., 2002. Hydrolysis of ATP by polymerized actin depends on the bound divalent cation but not profilin. Biochemistry 41, 597–602.

Bray, D., 2001. Cell Movements: From Molecules to Motility. Garland Publishing, New York.

Carlsson, A.E., 2005. The effect of branching on the critical concentration and average filament length of actin. Biophys. J. 89, 130–140.

Carlsson, A.E., 2006. Stimulation of actin polymerization by filament severing. Biophys. J. 90, 413–422.

Cooper, J.A., Buhle Jr, E.L., Walker, S.B., Tsong, T.Y., Pollard, T.D., 1983. Kinetic evidence for a monomer activation step in actin polymerization. Biochemistry 22, 2193–2202.

Dufort, P.A., Lumsden, C.J., 1993. High microfilament concentration results in barbed-end ADP caps. Biophys. J. 65, 1757–1766.

Einstein, A., 1956. Investigations on the Theory of Brownian Movement. Dover Publications, Inc., New York.

Ermentrout, G.B., Edelstein-Keshet, L., 1998. Models for the length distributions of actin filaments: II. Polymerization and fragmentation by gelsolin acting together. Bull. Math. Biol. 60, 477–503.

Frieden, C., Goddette, D.W., 1983. Polymerization of actin and actin-like systems: evaluation of the time course of polymerization in relation to the mechanism. Biochemistry 22, 5836–5843.

Fujiwara, I., Takahashi, S., Tadakuma, H., Funatsu, T., Ishiwata, S., 2002. Microscopic analysis of polymerization dynamics with individual actin filaments. Nat. Cell Biol. 4, 666–673.

Galkin, V.E., Orlova, A., VanLoock, M.S., Shvetsov, A., Reisler, E., Egelman, E.H., 2003. ADF/cofilin use an intrinsic mode of F-actin instability to disrupt actin filaments. J. Cell Biol. 163, 1057–1066.

Gibson, M.A., Bruck, J., 2000. Efficient exact stochastic simulation of chemical systems with many species and many channels. J. Phys. Chem. A 104, 1876–1889.

Gillespie, D.T., 1977. Exact stochastic simulation of coupled chemical-reactions. J. Phys. Chem. 81, 2340–2361.

Hill, T.L., 1983. Length dependence of rate constants for end-to-end association and dissociation of equilibrium linear aggregates. Biophys. J. 44, 285–288.

Howard, J., 2001. Mechanics of Motor Proteins and the Cytoskeleton. Sinauer Associates, Inc., Sunderland, MA.

Hu, J., Matzavinos, A., Othmer, H.G., 2006. A theoretical approach to actin filament dynamics. J. Stat. Phys. 128, 111–138.

Kas, J., Strey, H., Tang, J.X., Finger, D., Ezzell, R., Sackmann, E., Janmey, P.A., 1996. F-actin, a model polymer for semiflexible chains in dilute, semidilute, and liquid crystalline solutions. Biophys. J. 70, 609–625.

Kudryashov, D.S., Phillips, M., Reisler, E., 2004. Formation and destabilization of actin filaments with tetramethylrhodamine-modified actin. Biophys. J. 87, 1136–1145.

Kuhn, J.R., Pollard, T.D., 2005. Real-time measurements of actin filament polymerization by total internal reflection fluorescence microscopy. Biophys. J. 88, 1387–1402.

Limozin, L., Barmann, M., Sackmann, E., 2003. On the organization of selfassembled actin networks in giant vesicles. Eur. Phys. J. E Soft Matter 10, 319–330.

Marques, C., Turner, M., Cates, M., 1994. Relaxation mechanisms in worm-like micelles. J. Non-Crystalline Solids 172, 1168–1172.

Oosawa, F., Asakura, S., 1975. Thermodynamics of the Polymerization of Protein. Academic Press, Inc., New York, NY.

Orlova, A., Shvetsov, A., Galkin, V.E., Kudryashov, D.S., Rubenstein, P.A., Egelman, E.H., Reisler, E., 2004. Actin-destabilizing factors disrupt filaments by means of a time reversal of polymerization. Proc. Natl. Acad. Sci. USA 101, 17664–17668.

Pieper, U., Wegner, A., 1996. The end of a polymerizing actin filament contains numerous ATP-subunit segments that are disconnected by ADP-subunits resulting from ATP hydrolysis. Biochemistry 35, 4396–4402.

Pollard, T.D., 1986. Rate constants for the reactions of ATP- and ADP-actin with the ends of actin filaments. J. Cell. Biol. 103, 2747–2754.

Pollard, T.D., Borisy, G.G., 2003. Cellular motility driven by assembly and disassembly of actin filaments. Cell 112, 453–465.

Pollard, T.D., Blanchoin, L., Mullins, R.D., 2000. Molecular mechanisms controlling actin filament dynamics in nonmuscle cells. Annu. Rev. Biophys. Biomol. Struct. 29, 545–576.

Sept, D., McCammon, J.A., 2001. Thermodynamics and kinetics of actin filament nucleation. Biophys. J. 81, 667–674.

Sept, D., Xu, J., Pollard, T.D., McCammon, J.A., 1999. Annealing accounts for the length of actin filaments formed by spontaneous polymerization. Biophys. J. 77, 2911–2919.

Stukalin, E.B., Kolomeisky, A.B., 2006. ATP hydrolysis stimulates large length fluctuations in single actin filaments. Biophys. J. 90, 2673–2685.

Tobacman, L.S., Korn, E.D., 1983. The kinetics of actin nucleation and polymerization. J. Biol. Chem. 258, 3207–3214.

VanDongen, P., Ernst, M., 1984. Kinetics of reversible polymerization. J. Stat. Phys. 37, 301–324.

Vavylonis, D., Yang, Q., O'Shaughnessy, B., 2005. Actin polymerization kinetics, cap structure, and fluctuations. Proc. Natl Acad. Sci. USA 102, 8543–8548.

Wegner, A., Savko, P., 1982. Fragmentation of actin filaments. Biochemistry 21, 1909–1913.

Supplemental Material

List of the modeled processes. We simulate explicitly the following processes (see Figure 1 and respective rates in Table 1):

1) Subunit addition to a trimer (nucleation of a filament);
2) Loss of a subunit from a tetramer (complete disassembly of a filament);
3) ATP-subunit addition to a filament's barbed or pointed end;
4) ATP-, ADP·P_i-, or ADP-subunit loss from a barbed or pointed end;
5) Random γ-phosphate hydrolysis on ATP-subunits within a filament;
6) Random γ-phosphate release from ADP·P_i-subunits within a filament;
7) Barbed-to-pointed end-to-end filament-filament annealing;
8) Random filament fragmentation (filament breaks in two at a random point with the rate proportional to its length);
9) Stress-induced filament fragmentation (filament breaks in two at a random point with the rate independent of its length but proportional to square of the average filaments' length).

Note that the actin monomer concentration is simulated explicitly, but all monomers are assumed to be in ATP-state: nucleotide replacement (ATP for ADP or ADP·P_i) is assumed to occur instantaneously once a subunit is in solution. The dimer and trimer concentrations are not simulated dynamically because of the rapid equilibration of these concentrations with the monomer concentration. Rather, actin dimer concentration is calculated assuming equilibrium with monomers, and then trimer concentration is calculated assuming equilibrium with dimers based on the known rate shown in Table 1.

Supplemental Figure 1. Validation of annealing and fragmentation versus published experimental data. Our model, implemented as described in Methods, was used to simulate an experiment carried out in Andrianantoandro, E., L. Blanchoin, D. Sept, J. A. McCammon, and T. D. Pollard. 2001. Kinetic mechanism of end-to-end annealing of actin filaments. J Mol Biol 312:721-730. Briefly, 0.5 μM actin was polymerized in the presence of phalloidin to eliminate monomer addition and loss from filaments. The filaments were then mechanically sheared to an average length less than 0.5 micrometers, after which they were sampled, and the length distribution characterized by light microscopy, at various time points over 24 hours. We simulated the presence of phalloidin by reducing all subunit off-rates to zero, and mechanical shearing by increasing the random fragmentation rate constant by 10 orders of magnitude until the desired average length was achieved. Simulated distributions (*gray '+'*) matched the measured distributions closely (*black lines*; data provided by Ernesto Andrianantoandro).

Supplemental Figure 2. Effects of assuming instantaneous nucleotide exchange on G-actin monomers. In order to check this assumption, which was used for all results in the main body of the paper, we performed hybrid simulations of stochastic filament-related events (nucleation, subunit addition/loss, annealing, fragmentation) in parallel with numerical solution of differential equations describing nucleotide exchange (ATP for ADP) on G-actin, on novel model results. A rate constant of 0.009 s^{-1} for nucleotide exchange (ATP for ADP) on G-actin was used (5), and the time interval for calculation of concentration changes was 0.01 seconds. (*A*) Polymerization curve for a 3.0 μM total

actin simulation over 24 hours (86400 seconds); ATP-G-actin (*red line*) and ADP-G-actin (*green line*). The critical concentration was ~0.138 μM, as opposed to ~0.140 μM, and the time course of polymerization was qualitatively similar to those of simulations in which instantaneous exchange of ATP for ADP was assumed (see Figure 2A, Supplemental Movies 1-3). With instantaneous exchange, ATP-G-actin decreased from 3.0 to less than 0.15 μM in 51 ± 2 minutes, whereas with hybrid stochastic simulation of filament events and numerical solution of nucleotide turnover (this figure), ATP-G-actin decreased from 3.0 to less than 0.15 μM in 47 ± 1 minute (N = 3 for each type of simulation, mean ± sem). (*B*) Distribution of bound nucleotides in the barbed end terminal micrometer. These distributions closely match those from straight stochastic simulations (Figure 5B). (*C*) Length excursions at the barbed end between 4000 and 5800 seconds for 3.0 μM total actin. The distribution of these growth (positive) and shrinking (negative) excursions appears no different from that for simulations without ADP-G-actin accounted for.

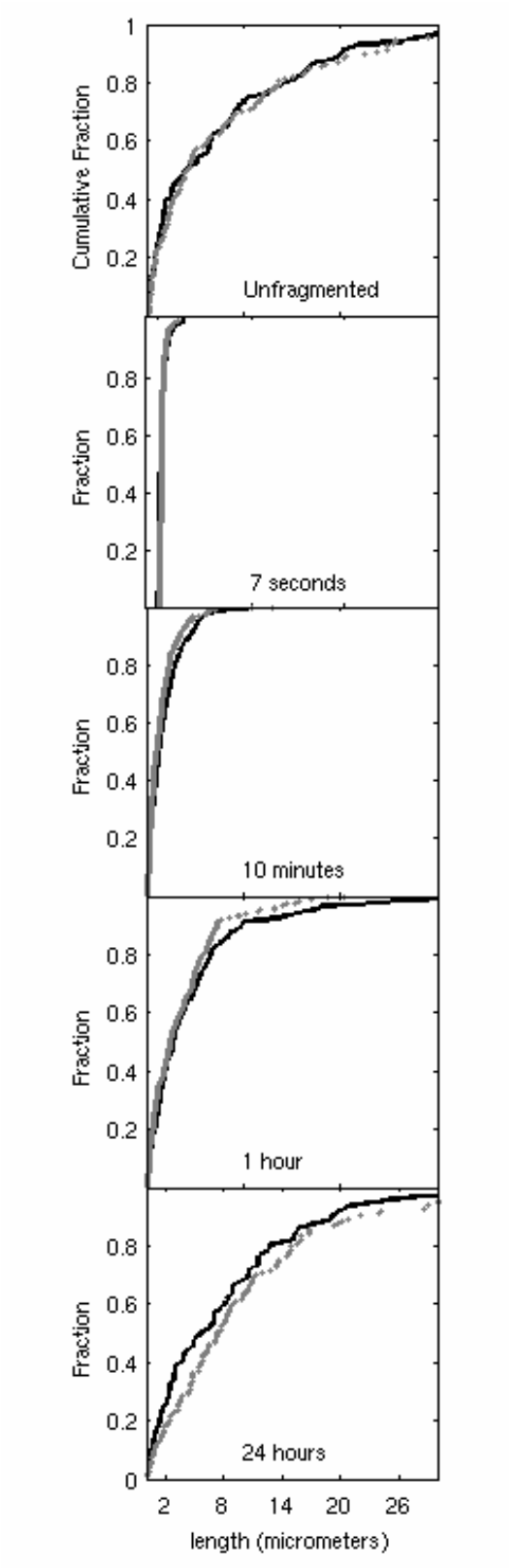

Supplemental Figure 1

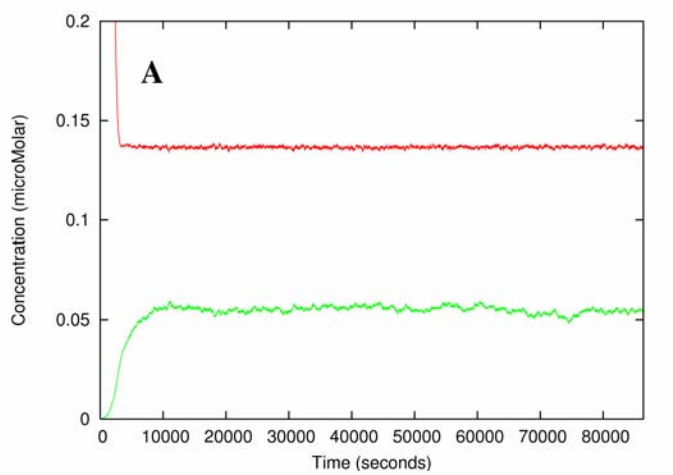

Supplemental Figure 2 (A)

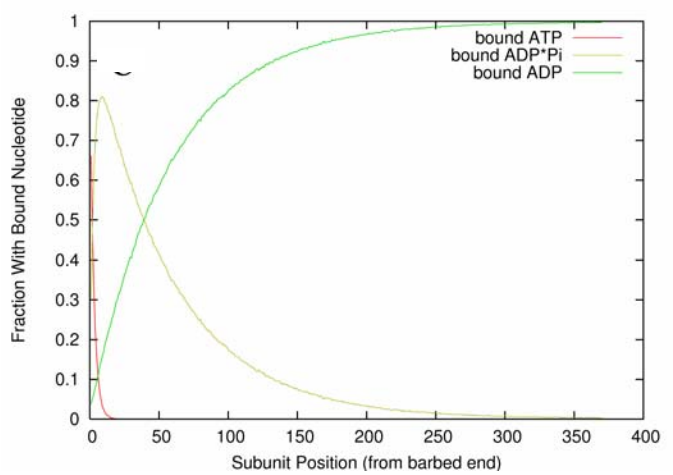

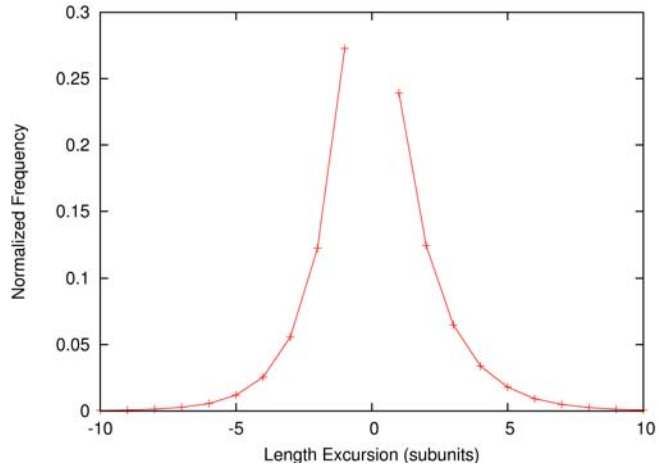

Supplemental Figure 2 (B, C)